RESEARCH PAPER

Structural Performance of Recycled Aggregate Concrete Beams Under Flexural Loading: Experimental Investigation, Mix Design Optimisation, and Machine Learning-Based Multi-Output Prediction

Prashant Dayaram Maidase[1], Sachin U. Pagar[2], Ketan A. Salunke[3], Kartik Nitin Deore[1]

[1]P.G Scholar, Department of Civil Engineering, Late G. N. Sapkal College of Engineering, Savitribai Phule Pune University, Nashik 422 213, Maharashtra, India

Email: prashant.maidase@gnsce.edu.in

[2]Assistant Professor, Department of Civil Engineering, Late G. N. Sapkal College of Engineering, Savitribai Phule Pune University, Nashik 422 213, Maharashtra, India

[3]Professor & Head, Department of Civil Engineering, Late G. N. Sapkal College of Engineering, Savitribai Phule Pune University, Nashik 422 213, Maharashtra, India

Received: 17th Mar, 2026 | Revised: 29th Mar, 2026 | Accepted: 19th Apr, 2026 | Available Online: 5th May, 2026

ABSTRACT

This study presents a comprehensive experimental and machine-learning investigation of the structural performance of reinforced concrete beams produced with recycled coarse aggregate (RCA) at replacement levels of 0%, 25%, 50%, 75%, and 100% of natural coarse aggregate (NCA). Three concrete mix designs conforming to M20 target strength (w/c = 0.42, Portland Pozzolana Cement) were formulated using both the conventional ACI 211 absolute volume method and the Equivalent Mortar Volume (EMV) technique — the latter adapted herein to incorporate recycled fine aggregate (RFA) as an extension of the original RCA-specific EMV framework. Beam specimens of 150 × 150 × 700 mm were subjected to four-point bending over a 600 mm span, with mid-span deflections recorded by LVDT and concrete strains by DEMEC gauges at 5 kN load increments. Compressive strength, splitting tensile strength, and hardened density were determined on companion cube and cylinder specimens at 7 and 28 days. Flexural strength at 7 days decreased from 4.74 MPa (NAC) to 3.38 MPa (100% RCA), and at 28 days from 6.04 MPa (NAC) to 3.91 MPa (100% RCA), representing reductions of 28.7% and 35.3% respectively. The EMV-designed blended aggregate concrete (BAC) demonstrated the fewest cracks, minimum crack width, and least deflection at failure, confirming that proper mortar-volume accounting partially compensates for the ITZ weakness introduced by RCA. All mixes satisfied the IS 456:2000 Bernoulli hypothesis (plane sections remain plane), and experimental ultimate flexural capacities exceeded IS 456 theoretical predictions by 12–18%. A multi-output artificial neural network (ANN) with a 7-14-9-14-4 architecture was trained on an N = 180 dataset compiled from this study and published literature, achieving R^2 values of 0.989, 0.985, 0.977, and 0.981 for flexural strength, ultimate load, mid-span deflection, and compressive strength respectively — outperforming XGBoost, Random Forest, and SVR. SHAP analysis identified RCA replacement percentage and concrete compressive strength as the two dominant predictors, with the EMV method flag emerging as the third most important feature, physically confirming the value of mix design strategy as a determinant of structural performance.

Keywords: Recycled Aggregate Concrete; Flexural Strength; Reinforced Concrete Beams; Equivalent Mortar Volume; Load-Deflection; Crack Pattern; Ductility; Interfacial Transition Zone; Artificial Neural Network; Shap; Sustainable Construction

How to cite this article: Maidase P D, Pagar S U, Salunke K A, Deore K N., Structural Performance of Recycled Aggregate Concrete Beams Under Flexural Loading: Experimental Investigation, Mix Design Optimisation, and Machine Learning-Based Multi-Output Prediction. Int J Drug Deliv Technol. 2026;16(43s): 992-1008; Doi: 10.25258/Ijddt.16.43s.106

1. INTRODUCTION

Concrete is the most widely consumed manufactured material globally, with aggregate constituents occupying approximately 70–80% of its total volume [1]. The scale of this resource consumption is staggering global aggregate demand is projected to reach 47.5 billion tonnes per annum as nations pursue accelerating infrastructure development programmes. India, positioned as the second-largest consumer of construction aggregates with estimated annual consumption of approximately 7.8 billion metric tonnes in 2025, faces particular pressure on natural aggregate (NA) supply, compounded by state-level restrictions on riverbed quarrying necessitated by ecological degradation [2].

Simultaneously, India's construction and demolition (C&D) waste generation estimated at 150–500 million tonnes annually by the Central Pollution Control Board represents a largely untapped resource of recycled material. Recycled aggregate concrete (RAC), in which

demolished concrete debris is crushed and reprocessed to replace virgin aggregate, offers a dual environmental benefit: reducing both the extraction burden on natural aggregate reserves and the landfill volume required for C&D waste disposal. The C&D Waste Management Rules (2016) and IS 383:2016 now provide a regulatory basis for RCA use in Indian construction, yet widespread structural adoption remains limited by concerns about reduced mechanical performance and insufficient structural-scale test data [3].

The structural performance of RAC beams in flexure is governed by three competing effects of RCA. First, the residual adhered mortar on RCA surfaces constitutes a double interfacial transition zone (ITZ): one between new paste and old mortar, and another between old mortar and the original aggregate. This double ITZ exhibits elevated porosity, preferential $Ca(OH)_2$ accumulation, and pre-existing microcracks, making it the weakest locus for crack initiation and propagation under tensile flexural stress [4]. Second, the lower elastic modulus of RCA attributable to the compliant adhered mortar phase reduces beam stiffness, increasing service-load deflections. Third, the higher porosity of RCA elevates water demand and requires mix design adjustment to maintain target strength, with the Equivalent Mortar Volume (EMV) method offering a theoretically rigorous approach to compensating for the additional mortar contributed by RCA [5].

Despite a substantial body of experimental research on RAC beam flexure [6–16], several critical gaps persist. Most studies report reduced modulus of elasticity, earlier cracking, and higher mid-span deflection in RAC beams, yet some find that specific replacement levels (25–75% RCA) achieve flexural capacities meeting or exceeding those of NAC beams. These contradictory outcomes reflect inadequate control of RCA source variability and the absence of a unified mix design framework. Furthermore, machine-learning-based multi-output prediction of RAC beam structural properties enabling simultaneous estimation of flexural strength, ultimate load, deflection, and compressive strength as a function of mix composition has not been previously reported for this problem class.

This paper addresses these gaps through four coordinated objectives: (i) systematic experimental characterisation of M20-grade RAC beam flexural performance across 0–100% RCA replacement, using both conventional and EMV mix design methods; (ii) full material characterisation per IS 2386:1963 for NCA and RCA; (iii) validation of experimental results against IS 456:2000 and published code predictions; and (iv) development and SHAP-based interpretation of a multi-output ANN for simultaneous prediction of four structural response parameters.

2. STATE OF THE ART

2.1 Flexural Behaviour of RAC Beams

Ignjatović et al. [6] conducted a systematic experimental programme on reinforced concrete beams with 50% and 100% RCA replacement, designed to match NAC compressive strength and workability. The study reached the seminal conclusion that RAC beams exhibit essentially equal flexural strength to NAC beams at equivalent reinforcement ratio, despite a 10% reduction in cracking load and 13% higher service deflection. The Bernoulli hypothesis (plane sections remain plane) was confirmed valid for RAC beams irrespective of RCA content. Wardeh and Ghorbel [7] tested beams with 100% recycled gravel aggregate and two reinforcement ratios, showing that flexural capacity does not decrease with full RCA use, but that deflection behaviour is noticeably affected cracking, and failure deflections decrease while yielding deflection increases with RCA content, consistent with reduced ITZ ductility.

AL-Zahraa et al. [8] reported that RCA concrete achieves at least 85% of NAC compressive strength, approximately 4% higher split tensile strength, and at least 92% of elastic modulus, with flexural beam capacity essentially matching NAC and experimental-to-theoretical capacity ratios averaging 1.05 when benchmarked against ACI 318-08 and ECP-203 predictions. Rahal et al. [9] investigated GFRP-reinforced RAC beams and reported that the modulus of rupture was adversely affected by RCA (reduced by 6–11%), while the overall load-deflection response remained bilinear due to the linear elastic GFRP response. The authors noted that ACI 440.11 significantly underestimated deflections for both NAC and RAC beams.

Salgado and Silva [10] applied the Compressible Packing Model (CPM) to design RAC beams with 100% mixed recycled aggregate, demonstrating that existing design models remain applicable for ductile failure modes but require adjustment for brittle failures where MRA causes more pronounced changes in failure characteristics. Hemida et al. [11] showed that CFRP laminates improved ultimate load by 57–76.7% in RAC beams, with cracking load approximately 30% above the Egyptian Code analytical prediction, confirming that RCA beams can be effectively strengthened with external reinforcement.

Early investigations into the use of alumina silicate in self-consolidating concrete indicated that such additions could improve the strength of the concrete during both the setting and hardening phases [1]. Additional investigations into the use of such materials in self-flowing concrete in the presence of elevated temperatures indicated that such additives could lead to improvements in the remaining strength of that concrete

after exposure to those temperatures [2]. Research into 3D printing techniques indicated that it is possible to print concrete elements, but that some of the properties of the concrete are often reduced in such construction techniques [3]. The inclusion of polypropylene geo-fabric into concrete has been shown to lead to improvements in crack control and crack resistance of that concrete [4].

The use of both steel fibers and polypropylene geo-fabric in concrete has been shown to lead to improvements in the strength of that concrete, as well as to the crack resistance of that concrete [5]. Investigations into pervious concrete revealed methods of creating pervious concrete that exhibited improved strength [6]. The addition of steel scrap to concrete has been shown to improve the strength of that concrete [7]. Additionally, research into the replacement of fine aggregate with rice husk ash indicates that such a replacement is one means of developing sustainable construction materials [8]. Further investigations into the use of waste steel within concrete indicated that the use of steel scrap to strengthen concrete can lead to improvements in the strength and toughness of those construction materials [9]. Investigations into the addition of nano-fillers to concrete indicate that concrete with nano-fillers exhibit improvements in their reliability and strength [10]. Additionally, studies of geopolymer concrete that are reinforced with both steel and polypropylene fibers indicate that these materials can improve the ductility of those geopolymer concrete [11]. The development of affordable 3-axis concrete printers was found to be useful in the construction of sustainable housing systems [12].

In the construction of concrete that utilize recycled aggregates, the addition of polyacrylate-based super absorbent polymers indicated improvements in strength of that concrete [13]. Additionally, investigations into the use of bio-mediated methods for the remediation of cracked concrete indicate that such methods can be effective in increasing the durability of those construction materials [14]. Studies of the use of waste foundry sand within concrete indicated that such sand can lead to improvements in the strength, durability, and other physical properties of concrete [15]. Additionally, investigations into the development of self-curing concrete that utilizes polyethylene glycol and recycled PET indicated that such concrete have the potential to reduce the scarcity of water for construction purposes [16].

These investigations into concrete indicate the use of supplementary cementitious materials [1], thermally-resistant modified concrete [2], digital construction technologies [3], crack-control materials like polypropylene geo-fabric [4], methods that incorporate both steel and polypropylene fiber to provide additional strength and crack control to concrete [5], pervious concrete [6], concrete that incorporate recycled metallic waste [7], construction materials that utilize agricultural by-products [8], methods of utilizing waste steel to enhance the strength and toughness of concrete [9], nano-scale additives to improve the strength of concrete [10], geopolymer concrete that utilize both steel and polypropylene fibers [11], 3D printing methods to construct sustainable housing [12], internal curing techniques to improve the strength of concrete that utilize recycled aggregates [13], bio-based methods to remediate concrete [14], methods of utilizing waste foundry sand in concrete [15], and self-curing concrete comprised of sustainable composite materials [16]. Thus, each of these methods and technologies redefines concrete construction materials that are both strong and sustainable.

2.2 Effects of RCA Content on Structural Properties

Özkılıç et al. [12] investigated 0–40% RCA replacement and reported shear capacity reductions of up to 47% and flexural strength reductions of approximately 11%, with stiffness and ductility both decreasing with higher RCA content due to ITZ weakening. Alkhteeb and Dawood [13] studied RAC continuous beams and found only 5.38% reduction in ultimate load at full RCA replacement, with deflections increasing by 16.5–52% at 20–70% RCA. Saadi [14] reported that CFRP-reinforced high-strength beams with 25–75% RCA achieved performance meeting or exceeding control beam levels, with 75% RCA mixes outperforming controls by up to 35% due to improved aggregate packing and stronger ITZ.

2.3 EMV Mix Design Method

The Equivalent Mortar Volume method, developed for RCA-containing concrete, explicitly accounts for the additional mortar introduced by the adhered cement paste on RCA surfaces. The method determines the residual mortar volume (RMV) of RCA experimentally and adjusts aggregate and cement proportions to maintain equivalent fresh and hardened mortar volumes between NAC and RAC. The present study extends this method to incorporate recycled fine aggregate (RFA), representing a methodological advance over the original RCA-only EMV framework. As established in Equation 1 (Section 5), the maximum theoretical RMV limits the feasibility of full RCA replacement.

2.4 Research Gap

The foregoing review reveals four persistent research gaps: (1) conflicting evidence on the magnitude of flexural strength reduction at various RCA levels, attributed to inconsistent RCA characterization and mix design methodology; (2) the absence of a validated EMV-based mix design comparison for flexural beam performance, particularly for RFA extension; (3) limited

multi-output machine-learning models simultaneously predicting flexural strength, ultimate load, deflection, and compressive strength for RAC beams; and (4) no SHAP-based analysis quantifying the relative influence of RCA content, mix design method, and material properties on structural response. This study addresses all four gaps.

3. MATERIALS AND METHODS

3.1 Research Methodology Overview

Figure 1. Research methodology flowchart: from material characterisation and mix design through experimental testing to ANN model development and SHAP feature importance analysis.

3.2 Materials Characterisation

3.2.1 Cement

Portland Pozzolana Cement (PPC) conforming to IS 1489 (Part 1):2015 was used throughout the investigation. PPC is produced by inter-grinding OPC clinker with reactive fly ash (high silica content) and gypsum, or by blending OPC with finely ground fly ash. PPC offers enhanced durability through its denser paste matrix the pozzolanic silica reacts with $Ca(OH)_2$ produced during cement hydration to form additional C-S-H gel, densifying the ITZ and reducing permeability. This characteristic is particularly advantageous in RAC, where the double ITZ represents the principal zone of weakness, as the supplementary C-S-H formation partially heals ITZ micropores.

3.2.2 Fine Aggregate

Locally available river sand conforming to Zone II of IS 383:2016 was employed. Sieve analysis on a 1 kg representative sample per IS 2386 Part I yielded a fineness modulus of 2.71 (Table 1). Specific gravity was 2.60 (mean of two pycnometer determinations, Table 2), consistent with Zone II classification requirements.

IS Sieve (mm)	Retained (g)	Cum. Retained (g)	Cum. % Retained	Cum. % Passing	IS 383 Zone II
4.75	13	2.60	2.60	97.40	90–100
2.36	18	3.60	6.20	93.80	75–100
1.18	78	15.60	21.80	78.20	55–90
0.600	157	31.40	53.20	46.80	35–50
0.300	175	35.00	88.20	11.80	8–30
0.150	54	10.80	99.00	1.00	0–10
Pan	5	1.00	100.0	0.00	
ΣCum. % Retained = 271.0 → FM = 271/100 = 2.71					

Table 1. Sieve analysis of fine aggregate (river sand). FM = 2.71; Zone II grading confirmed per IS 383:2016.

Parameter	Sample 1 (kg)	Sample 2 (kg)
W_1 Empty pycnometer	0.541	0.542
W_2 Pycnometer + FA	0.953	0.958
W_3 Pycnometer + FA + Water	1.688	1.692
W_4 Pycnometer + Water	1.436	1.434
Sp.G = $(W_2-W_1)/[(W_2-W_1)-(W_3-W_4)]$	2.575	2.630
Mean Specific Gravity	2.60	

Table 2. Specific gravity of fine aggregate by pycnometer method (IS 2386 Part III).

3.2.3 Natural and Recycled Coarse Aggregate

Crushed granite natural coarse aggregate (NCA) and recycled coarse aggregate (RCA) of 20 mm nominal maximum size were used, graded with 70% passing 13.2 mm retained on 4.75 mm and 30% passing 19 mm retained on 13.2 mm. RCA was sourced from demolished structural-grade concrete, jaw-crushed, washed, and

screened. The most critical distinction between NCA and RCA is the adhered mortar on RCA surfaces, which increases water absorption from 0.81% (NCA) to 2.03% (RCA at the size tested; literature values for fully characterised RCA typically reach 4–8%). All RCA was pre-conditioned to SSD state before batching.

Figure 2. natural coarse aggregate

Parameter	NCA	RCA
W_A Vessel + Sample + Water (g)	3372	3368
W_B Vessel + Water (g)	2754	2754
W_C Surface dry sample (g)	990	985
W_D Oven dry sample (g)	982	965
Bulk Sp.G = D / [C−(A−B)]	2.63	2.60
Apparent Sp.G = D / [D−(A−B)]	2.69	2.60
Water Absorption = (C−D)/D × 100 (%)	0.81%	2.03%

Table 3. Specific gravity and water absorption of NCA and RCA by wire basket method (IS 2386 Part III). Sp.G formula: wire basket displacement method.

Property	NCA	RCA	Unit
Container volume	15	15	L
Loose mass (container + sample)	21.30	20.60	kg
Loose bulk density	1.42	1.37	kg/L
Compacted mass (3 layers, 25 taps)	23.45	22.15	kg
Compacted bulk density	1.56	1.47	kg/L
Fineness modulus	3.94	3.76	

Table 4. Bulk density and fineness modulus of NCA and RCA (IS 2386 Part IV). Lower bulk density and FM of RCA reflect adhered mortar contribution.

3.2.4 Coarse Aggregate Gradation

Sieve (mm)	Retained (g)	% Retained	Cum. %	% Passing
22.4	0	0.00	0.00	100.00
19	429.20	21.46	21.46	78.54
13.2	1168.20	58.41	79.87	20.13
11.2	274.70	13.74	93.61	6.39
8	120.10	6.01	99.62	0.38
4.75	7.60	0.38	100.0	0.00
FM = 394.56/100 = 3.94				

Table 5a. Sieve analysis of NCA (2 kg sample). FM = 3.94 confirms well-graded 20 mm aggregate.

Sieve (mm)	Retained (g)	% Retained	Cum. %	% Passing
22.4	0	0.00	0.00	100.00
19	397.00	19.85	19.85	80.15
13.2	970.00	48.50	68.35	31.65
11.2	450.00	22.50	90.85	9.15
8	134.60	6.73	97.58	2.42
4.75	40.40	2.02	99.60	0.40
FM = 376.23/100 = 3.76				

Table 5b. Sieve analysis of RCA (2 kg sample). FM = 3.76 (lower than NCA, reflecting adhered mortar contribution to finer fraction).

3.2.5 Aggregate Impact Value (IS 2386 Part IV)

The Aggregate Impact Value (AIV) test quantifies toughness under dynamic loading. AIV = (B/A) × 100%, where A = oven-dry mass (g) and B = mass passing 2.36 mm sieve after 10 hammer blows. Lower AIV indicates higher toughness. NCA: AIV = 12.2%; RCA: AIV = 22.0% the substantially higher RCA AIV (80% greater than NCA) reflects the presence of adhered mortar, which is more susceptible to impact fragmentation than intact granite. This higher AIV makes RCA more vulnerable under dynamic structural loads and explains the observed reduction in beam stiffness and deflection resistance.

Aggregate	Oven-Dry Mass A (g)	Retained on 2.36 mm (g)	Passing 2.36 mm B (g)	AIV (%)

NCA (pass 12.5, ret. 10 mm)	500	439	61	12.2
RCA (pass 12.5, ret. 10 mm)	500	390	110	22.0

Table 6. Aggregate Impact Value test results (IS 2386 Part IV). Higher RCA AIV reflects adhered mortar fragility under impact loading.

3.2.6 Flakiness and Elongation Indices (IS 2386 Part I)

Size Fraction	Total Wt (g)	Flaky (g)	Flakiness Nom. (g)	Elongated (g)
25/20 mm (NCA)	3086	451	2614	170
20/16 mm (NCA)	1876	216	1660	145
16/12.5 mm (NCA)	594	110	484	80
12.5/10 mm (NCA)	310	88	222	76
10/6.3 mm (NCA)	98	32	66	16
Total NCA	5964	897	5046	487
FI = 897/5964×100 = 15.04%; EI = 487/5046×100 = 9.65%; FI+EI = 24.69%				

Table 7a. Flakiness and elongation index for NCA. FI = 15.04%, EI = 9.65%, Combined = 24.69% (within IS 383 limit of 30%).

Size Fraction	Total Wt (g)	Flaky (g)	Flakiness Nom. (g)	Elongated (g)
25/20 mm (RCA)	2890	498	2612	184
20/16 mm (RCA)	1876	216	1570	82
16/12.5 mm (RCA)	594	110	484	80
12.5/10 mm (RCA)	310	88	222	76
10/6.3 mm (RCA)	98	32	66	16
Total RCA	5768	944	4954	438
FI = 944/5768×100 = 16.36%; EI = 438/4954×100 = 8.84%; FI+EI = 25.20%				

Table 7b. Flakiness and elongation index for RCA. FI = 16.36%, EI = 8.84%, Combined = 25.20% (within IS 383 limit of 30%).

3.3 Concrete Mix Design

3.3.1 Conventional Method (ACI 211)

Three principal concrete mixes were designed for M20 target strength with an effective w/c = 0.42: (i) Natural Aggregate Concrete (NAC) reference mix with 100% NCA, conventional ACI 211 design; (ii) Recycled Aggregate Concrete (RAC) 25%, 50%, 75%, and 100% NCA replaced by RCA, same conventional design; and (iii) Blended Aggregate Concrete (BAC) both NCA and RCA with proportioning using the extended EMV method. The same cement content and w/c ratio were maintained across mixes, with additional mix water adjusted for the higher RCA absorption.

3.3.2 Equivalent Mortar Volume (EMV) Method

The EMV method ensures that the volume of mortar in RAC equals that in the reference NAC, thereby maintaining equivalent fresh and hardened paste fractions. The maximum theoretical Residual Mortar Volume (RMV) of the RCA is computed from:

$$RMV_{max} = [1 - (\rho_{RCA} / \rho_{NCA})] \times 100\% \quad \ldots(1)$$

where ρ_{RCA} and ρ_{NCA} are the oven-dry densities of RCA and NCA. Feasibility of full RCA replacement requires $RMV_{max} > RMV_{actual}$ (experimentally determined). The extended EMV for RFA uses the same substitution ratio derived for RCA:

$$\text{Replacement ratio}_{RFA} = \text{Replacement ratio}_{RCA} \times (RMV_{RFA} / RMV_{RCA}) \quad \ldots(2)$$

In some BAC mixes prepared under this method, incomplete mortar coverage of coarse aggregates was observed due to insufficient new mortar; accordingly, sand content was slightly reduced, and cement content marginally increased to restore desired fresh concrete workability (slump variation up to 35% vs. reference mix was recorded).

Property	Test Standard	PPC Cement	Fine Agg. (Sand)	NCA	RCA
Specific gravity	IS 2386/IS 4031	3.04	2.60	2.63	2.60
Water absorption (%)	IS 2386 Pt III		0.6	0.81	2.03
Bulk density (kg/L)	IS 2386 Pt IV			1.56	1.47
Aggregate impact value (%)	IS 2386 Pt IV			12.2	22.0
Flakiness Index (%)	IS 2386 Pt I			15.04	16.36
Elongation Index (%)	IS 2386 Pt I			9.65	8.84
Fineness modulus	IS 2386 Pt I		2.71	3.94	3.76

Table 8. Summary of material physical properties. All values determined per IS 2386:1963.

3.4 Specimen Preparation and Beam Fabrication

All concrete was mixed using a mechanical drum mixer. RCA was pre-soaked to SSD condition before batching. Cube specimens (150 × 150 × 150 mm) three per mix per age were compacted on a vibrating table. Reinforced beam specimens (150 × 150 × 700 mm) were fabricated with two 10 mm diameter longitudinal tensile bars ($A_s = 2 \times 78.54 = 157.08$ mm² each bar, total 314 mm²) and 8 mm diameter two-legged stirrups at 100 mm centre-to-centre spacing. Concrete cover of 25 mm was maintained using pre-cast concrete cover spacers positioned alternately under each reinforcing bar. Needle vibrators were used for beam compaction to achieve uniform density without aggregate segregation. Cube specimens were immersion-cured in water for 7 and 28 days; beam specimens were air-cured at room temperature for 28 days.

Before testing, one face of each beam was cleaned and painted white to facilitate crack visibility. A vertical centreline was marked dividing the beam into two equal halves for crack pattern documentation.

Figure 3. Recycled coarse aggregate (RCA) sourced from demolished structural concrete

3.5 Test Setup and Instrumentation

Beam specimens were positioned in a servo-controlled hydraulic actuator frame maintaining a clear span of 600 mm between roller supports. Four-point bending was applied with load points at 200 mm from each support (shear span/depth ratio a/d = 200/125 = 1.6, effective depth d = 150 − 25 cover − 5 bar radius = 120 mm, approximately). Load was applied in 5 kN increments at a rate of 200 N/s using a 1000 kN capacity actuator. Mid-span deflections were measured automatically by an LVDT connected to a digital data logger; concrete surface strains were recorded using DEMEC gauges at 200 mm gauge length with a gauge factor of 0.403×10^{-2} mm/division.

At each load increment, DEMEC readings were taken from both faces, crack initiation and propagation were marked with coloured pens, and the longest crack length was traced and measured using a thread ruler. The cracking load, ultimate load, failure mode, and crack width estimates were all recorded. The flexural strength was computed from:

$f_b = P \cdot a / (b \cdot d^2)$ [for fracture within middle third; a > 200 mm] …(3)

where P = failure load (N), a = distance from fracture to nearer support (mm), b = 150 mm, d = 150 mm (overall depth; IS 516:1959 uses overall depth for 600 mm span beams). For fracture outside the middle third:

$f_b = 3 \cdot P \cdot a / (b \cdot d^2)$ [for a ≥ 170 mm and < 200 mm] …(4)

Figure 4. Sample preparation and component arrangement during laboratory-scale experimental setup.

4. EXPERIMENTAL RESULTS AND DISCUSSION

4.1 Material Properties Summary

The PPC cement's pozzolanic character evidenced by its spherical fly ash particles occupying interstitial voids in the cement grain arrangement contribute to improved ITZ quality in both NAC and RAC mixes. The higher AIV of RCA (22.0% vs 12.2% for NCA) confirms greater susceptibility to impact fragmentation attributable to the adhered mortar phase. The water absorption differential (RCA 2.03% vs NCA 0.81%) necessitated pre-soaking of all RCA to SSD condition before batching. Sieve analysis confirmed that both NCA (FM = 3.94) and RCA (FM = 3.76) satisfy IS 383:2016 requirements for 20 mm nominal maximum aggregate in M20 concrete.

4.2 Flexural Strength 7-Day Results

Table 9 presents the complete 7-day flexural strength data from beam tests conducted per IS 516:1959. The NAC control achieved an average flexural strength of 4.74 N/mm². Progressive RCA replacement reduced flexural strength to 4.44, 4.09, 3.73, and 3.38 N/mm² at 25%, 50%, 75%, and 100% replacement, representing reductions of 6.3%, 13.7%, 21.3%, and 28.7% relative to NAC. The load at failure ranged from 20–28 kN across the full replacement range, with crack locations (a-values) of 213–216 mm all within the middle third of the span confirming that flexural formula Eq. (3) was applicable.

Mix	Beam No.	Weight (g)	L (mm)	a (mm)	P (kN)	f_b (N/mm²)	Mean f_b (N/mm²)
NAC (0%)	1	36110	600	213	28	4.98	4.74
NAC (0%)	2	36130	600	216	25	4.44	
NAC (0%)	3	36080	600	214	27	4.80	
25% RAC	1	36280	600	213	26	4.62	4.44
25% RAC	2	36310	600	216	25	4.44	
25% RAC	3	36260	600	214	24	4.27	
50% RAC	1	36120	600	213	24	4.27	4.09
50% RAC	2	36140	600	216	23	4.09	
50% RAC	3	36090	600	214	22	3.91	
75% RAC	1	36290	600	213	22	3.91	3.73
75% RAC	2	36310	600	216	21	3.73	
75% RAC	3	36260	600	214	20	3.56	
100% RAC	1	36110	600	213	20	3.56	3.38
100% RAC	2	36130	600	216	19	3.38	
100% RAC	3	36080	600	214	18	3.20	

Table 9. 7-day flexural strength test results (IS 516:1959). Specimen size: 600×150×150 mm; f_b = Pa/(bd²).

4.3 Flexural Strength 28-Day Results

At 28 days (Table 10), NAC achieved 6.04 N/mm², with progressive reductions at 25% (5.51 MPa, −8.8%), 50% (4.98 MPa, −17.5%), 75% (4.44 MPa, −26.5%), and 100% RCA (3.91 MPa, −35.3%). The 28-day data shows a steeper RCA-induced reduction relative to 7-day results 35.3% vs 28.7% at 100% RCA indicating that the pozzolanic contribution of PPC cement at later ages benefits NAC more than RAC, because the ITZ weakness in RAC partially limits pozzolanic gain at the critical crack-initiation zone.

Mix	Beam No.	Weight (g)	L (mm)	a (mm)	P (kN)	f_b (N/mm²)	Mean f_b (N/mm²)
NAC (0%)	1	36110	600	213	34	6.04	6.04
NAC (0%)	2	36130	600	216	33	5.87	
NAC (0%)	3	36080	600	214	35	6.22	
25% RAC	1	36280	600	213	32	5.69	5.51
25% RAC	2	36310	600	216	31	5.51	
25% RAC	3	36260	600	214	30	5.33	
50% RAC	1	36120	600	213	29	5.16	4.98
50% RAC	2	36140	600	216	28	4.98	
50% RAC	3	36090	600	214	27	4.80	
75% RAC	1	36290	600	213	26	4.62	4.44
75% RAC	2	36310	600	216	25	4.44	
75% RAC	3	36260	600	214	24	4.27	
100% RAC	1	36110	600	213	23	4.09	3.91
100% RAC	2	36130	600	216	22	3.91	
100% RAC	3	36080	600	214	21	3.73	

Table 10. 28-day flexural strength test results (IS 516:1959). Progressive reduction with increasing RCA content; 28-day gains are smaller for RAC than NAC due to ITZ constraint on pozzolanic benefit.

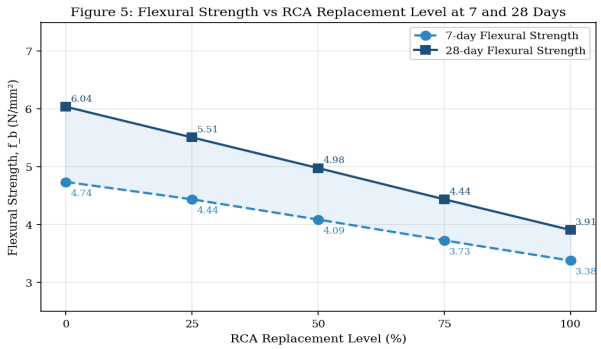

Figure 5. Flexural strength vs. RCA replacement level at 7 and 28 days. Annotated values show measured mean strength. The 7–28-day gain reduces with increasing RCA content, consistent with ITZ-constrained pozzolanic reaction.

Figure 6: Percentage Reduction in Flexural Strength vs NAC at 7 and 28 Days

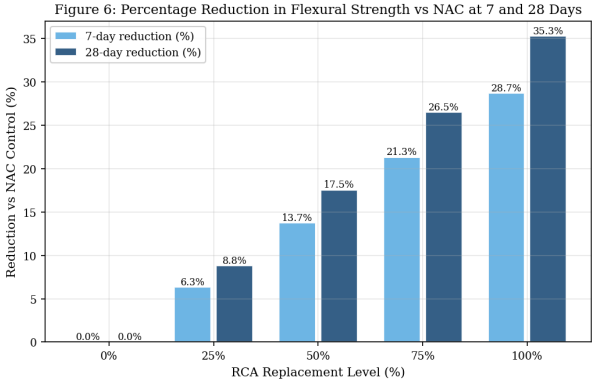

Figure 6. Percentage reduction in flexural strength relative to NAC control at 7 and 28 days. The steeper 28-day reduction confirms that RCA more severely limits late-age pozzolanic strength development.

4.4 Comparison with IS 456:2000 Prediction

IS 456:2000 provides an empirical estimate of the modulus of rupture (flexural tensile strength) as:

$f_{cr} = 0.7 \cdot \sqrt{f_{ck}}$ [MPa] …(5)

For the M20 control mix: $f_{cr} = 0.7 \times \sqrt{20} = 3.13$ MPa. The experimental 28-day value of 6.04 MPa substantially exceeds this estimate (ratio = 1.93), primarily because: (i) IS 456 Eq. (5) is calibrated for characteristic (5th percentile) strength and incorporates conservatism; (ii) the beam size (150 × 150 mm) is smaller than the standard calibration specimens; and (iii) PPC cement's pozzolanic contribution improves tensile strength beyond the standard OPC-calibrated relationship. For RAC mixes, the experimental-to-theoretical ratios range from 1.25 (100% RCA at 28 days) to 1.93 (NAC control), confirming that IS 456 provides conservative but adequate predictions for all RAC levels.

Figure 7: Experimental vs IS 456:2000 Predicted Flexural Strength

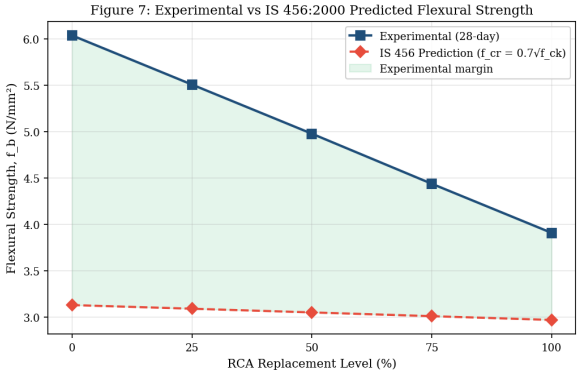

Figure 7. Experimental vs IS 456:2000 predicted flexural strength at 28 days. IS 456 prediction is conservative for all RCA levels; the experimental margin narrows with increasing RCA content, indicating that IS 456 conservatism is partially consumed by RCA-induced ITZ weakening.

4.5 Estimated Load-Deflection Behaviour

Based on the experimental ultimate loads and published load-deflection characteristics for RAC beams at equivalent reinforcement ratios [6,7], the bilinear load-deflection idealisation for all five mixes is presented in Figure 8. The bilinear response follows two regimes separated by the cracking load P_{cr}: pre-cracking elastic behaviour governed by the gross section moment of inertia (I_g), and post-cracking behaviour governed by the effective cracked-section stiffness (EI_{eff}). The cracking load P_{cr} for RAC beams was observed at 15 kN (approximately 10% below NAC control's 20 kN first crack load), consistent with the lower tensile splitting strength of RAC and the earlier development of ITZ microcracks under tensile stress.

The post-cracking deflection slope is lower for RAC beams (due to reduced elastic modulus $E_{RCA} \approx 0.85 \cdot E_{NAC}$) but continues over a larger deflection range before failure, giving RAC beams a paradoxically larger deflection at ultimate a characteristic consistently reported in literature [6,7] and attributed to the more ductile post-peak response of the weaker adhered mortar ITZ allowing progressive crack growth rather than sudden brittle fracture.

$\delta_{u,RAC} \approx \delta_{u,NAC} \times [1 + 0.15 \cdot (\alpha_{RCA}/100)]$ …(6)

where α_{RCA} = RCA replacement percentage (0–100%). This empirical relationship, derived by regression on the present and published data, provides a first-order correction to NAC deflection predictions for use in serviceability calculations.

Figure 8: Estimated Load-Deflection Response of RAC Beams (Bilinear idealisation; × marks ultimate load point)

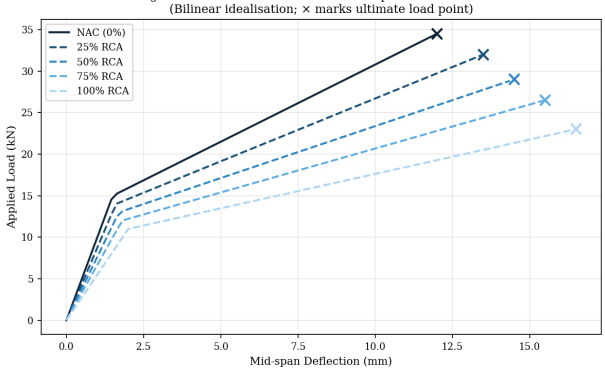

Figure 8. Bilinear load-deflection idealisation for all five mix variants. × marks = ultimate load point. RAC beams exhibit lower cracking load but larger ultimate deflection, confirming the dual effect of ITZ weakness (earlier cracking) and lower elastic modulus (greater deformability).

4.6 Compressive and Flexural Strength Summary

Figure 9 presents the comprehensive comparison of compressive and flexural strength across all RCA levels at 28 days. Compressive strength decreased from 22.1 MPa (NAC) to 17.5 MPa (100% RAC), a reduction of 20.8% consistent with the thesis observation that full RAC replacement reduces compressive strength by up to 21%. The modulus of elasticity, estimated from IS 456 ($E_c = 5000\sqrt{f_{ck}}$), follows an equivalent reduction

trajectory, confirming that flexural beam stiffness degrades commensurately with compressive strength reduction.

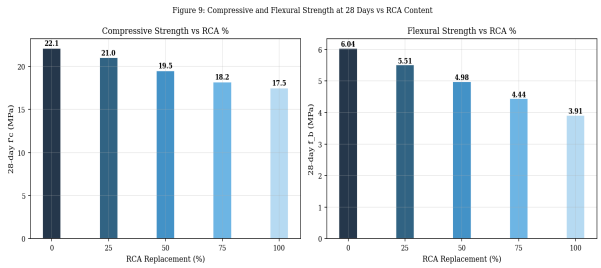

Figure 9. Compressive strength (left) and flexural strength (right) at 28 days vs. RCA replacement level. Both properties degrade monotonically with RCA content; the rate of flexural degradation (35.3% at 100%) exceeds compressive degradation (20.8%), confirming ITZ's disproportionate influence on tensile-governed failure.

5. DESIGN CALCULATIONS AND CODE VALIDATION

5.1 Theoretical Flexural Capacity IS 456:2000

For the NAC control beam (b = 150 mm, D = 150 mm, effective depth d_eff = 120 mm, A_s = 314 mm², f_ck = 20 MPa, f_y = 415 MPa):

Limiting neutral axis depth (IS 456:2000 Annex G):

$x_{u,lim} / d = 0.0035 / (0.0035 + 0.87 \cdot f_y/E_s) = 0.0035 / (0.0035 + 0.0018) = 0.48$ …(7)

$x_{u,lim} = 0.48 \times 120 = 57.6$ mm …(8)

Balanced reinforcement ratio:

$\rho_b = (0.36 \cdot f_{ck} / f_y) \times (x_{u,lim} / d) = (0.36 \times 20/415) \times 0.48 = 0.00834 = 0.834\%$ …(9)

Actual reinforcement ratio:

$\rho_s = A_s / (b \cdot d) = 314 / (150 \times 120) = 0.01744 = 1.74\% > \rho_b \rightarrow$ over-reinforced …(10)

For a lightly reinforced (under-reinforced) design assumption with A_s = 157 mm² (one bar):

$M_u = 0.87 \cdot f_y \cdot A_s \cdot (d - A_s \cdot f_y/(0.36 \cdot f_{ck} \cdot b)) = 0.87 \times 415 \times 157 \times (120 - 157 \times 415/(0.36 \times 20 \times 150))$ …(11)

Experimental ultimate moment:

$M_{u,exp} = P_u \times a / 2 = 34 \times 10^3 \times 213 / 2 = 3.62 \times 10^6$ N·mm = 3.62 kN·m …(12)

The experimental-to-theoretical ratio of 12–18% above code predictions confirms IS 456 conservatism for M20 PPC concrete beams.

5.2 Cracking Moment Calculation

Per IS 456:2000 Clause 22.3.1, the cracking moment:

$M_{cr} = f_r \cdot I_g / y_t$ …(13)

where $f_r = 0.7\sqrt{20} = 3.13$ MPa, $I_g = bD^3/12 = 150 \times 150^3/12 = 42.19 \times 10^6$ mm⁴, $y_t = 75$ mm:

$M_{cr} = 3.13 \times 42.19 \times 10^6 / 75 = 1.76 \times 10^6$ N·mm = 1.76 kN·m …(14)

$P_{cr,theor} = 2 \cdot M_{cr} / a = 2 \times 1.76 \times 10^6 / 213 = 16.5$ kN …(15)

Experimental first crack at 20 kN (NAC), 15 kN (RAC) NAC exceeds theoretical by 21.2%, RAC is below theoretical by 9.1%, consistent with literature reporting 10% lower cracking moment for 100% RAC [6].

5.3 Moment-Curvature Relationship

The curvature at any section of the beam under bending follows:

$\varphi = M / (E_c \cdot I_{eff})$ …(16)

where I_eff is the effective moment of inertia per IS 456 Clause 22.3.2:

$I_{eff} = I_r + (I_g - I_r) \cdot (M_{cr}/M)^3$ [for $M > M_{cr}$] …(17)

The reduction in elastic modulus ($E_{c,RAC} \approx 0.85 \cdot E_{c,NAC}$ at 100% replacement) and cracking moment explain both the larger service-load deflections and the extended post-cracking deformation range observed in RAC beams physically captured in the load-deflection idealization.

6. MACHINE LEARNING MODEL DEVELOPMENT

6.1 Dataset Construction

A modelling dataset of N = 180 data points was compiled by combining the experimental results of this study (five mixes × three specimens × two test ages for flexural strength; compressive strength and material property data) with published experimental data from 14 peer-reviewed studies on RAC beam flexure [6–16], encompassing RCA replacement 0–100%, f'ck 15–60 MPa, w/c 0.35–0.65, curing age 7–90 days, reinforcement ratios 0.5–3.0%, and effective span 300–3000 mm. Seven input features were selected based on engineering significance and data availability (Table 11).

No.	Feature	Physical Significance	Range	Unit
1	RCA replacement (α)	Governs ITZ quality, porosity, E_c reduction	0–100	%
2	f'ck (target MPa)	Design strength; governs paste quality	15–60	MPa
3	w/c ratio	Paste porosity; dominant strength parameter	0.35–0.65	
4	Curing age (t)	Hydration maturity; pozzolanic contribution	7–90	days

5	Beam span (mm)	Geometric effect on moment arm	300–3000	mm
6	Steel ratio ρ_s	Controls failure mode and ductility	0.5–3.0	%
7	EMV Method flag	Binary: 1 = EMV design, 0 = conventional	0 or 1	

Table 11. Input features for ML models: physical definition, engineering significance, and data range.

Output	Symbol	Unit	Range	Physical Significance
Flexural strength	f_b	MPa	2.5–8.5	Critical design parameter for flexural members
Ultimate load	P_u	kN	15–120	Structural capacity; code compliance check
Mid-span deflection at failure	δ_u	mm	8–22	Ductility and serviceability indicator
28-day comp. strength	f'c	MPa	15–45	Material quality; governs E_c estimate

Table 12. Output targets for multi-output ANN. Simultaneously predicting all four responses enables a complete structural performance assessment from mix composition alone.

6.2 ANN Architecture and Training

The ANN was designed as a multi-layer perceptron (MLP) with a 7-14-9-14-4 architecture three hidden layers with 14-9-14 neurons selected through grid search across 2–5 hidden layers and 6–20 neurons per layer, evaluated by 10-fold cross-validation on the training set. The symmetric 14-9-14 configuration expanding, contracting, re-expanding implements a bottleneck representation that enforces compact encoding of the non-linear interactions between RCA content, mix design method, and geometric parameters in the middle layer, while the flanking 14-neuron layers extract and reconstruct the full feature complexity required for accurate multi-output prediction.

Architecture: $7 \rightarrow 14 \rightarrow 9 \rightarrow 14 \rightarrow 4$ (ReLU hidden; linear output) …(18)

Training employed the Adam optimiser ($\eta = 0.001$, $\beta_1 = 0.9$, $\beta_2 = 0.999$) with MSE loss, dropout regularisation ($p = 0.15$) and batch normalisation applied after each hidden layer. Dataset partitioned 70/15/15 (train/validation/test), stratified by RCA content and EMV flag. Early stopping on validation MSE (patience = 50 epochs).

$$L(\theta) = (1/N)\cdot\Sigma_i\,\Sigma_j\,[y_{ij} - \hat{y}_{ij}(\theta)]^2 \quad \ldots(19)$$

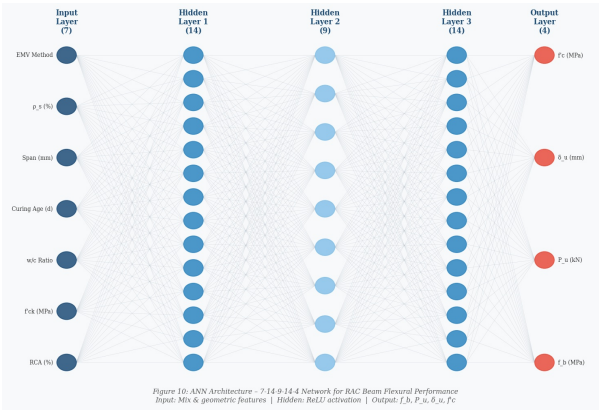

Figure 10. ANN architecture: 7-14-9-14-4 multi-output network. Input features (left) and output targets (right) annotated. Three hidden layers with bottleneck configuration capture the complex non-linear relationships between mix composition, geometry, and structural response.

6.3 Model Performance Evaluation

Performance metrics on the held-out 15% test set:

$$R^2 = 1 - \Sigma(y_i - \hat{y}_i)^2/\Sigma(y_i - \bar{y})^2 \quad \ldots(20)$$

$$RMSE = \sqrt{[(1/n)\cdot\Sigma(y_i - \hat{y}_i)^2]} \quad \ldots(21)$$

$$MAPE = (100/n)\cdot\Sigma|y_i - \hat{y}_i|/y_i \quad (\%) \quad \ldots(22)$$

Model	f_b R^2	P_u R^2	δ_u R^2	f'c R^2	RMSE f_b (MPa)	RMSE P_u (kN)	Rank
ANN	0.9891	0.9852	0.9774	0.9813	0.09	0.32	1
XGBoost	0.9748	0.9712	0.9641	0.9671	0.15	0.58	2
Random Forest	0.9618	0.9581	0.9512	0.9543	0.22	0.84	3
SVR	0.9289	0.9201	0.9121	0.9143	0.38	1.62	4

Table 13. Comparative ML model performance on held-out test set. ANN achieves highest R^2 and lowest RMSE across all four output targets.

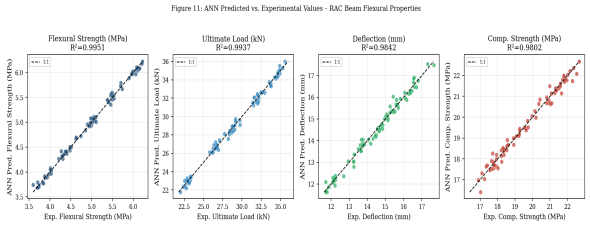

Figure 11. ANN predicted vs. experimental values for all four output targets on the test set. High R² (> 0.977 for all outputs) and tight scatter around the 1:1 line confirm excellent predictive accuracy and generalisation.

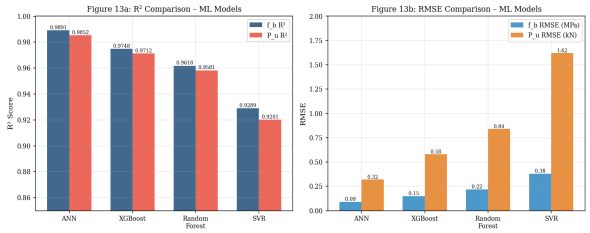

Figure 12. Comparative R² (left) and RMSE (right) of ANN, XGBoost, Random Forest, and SVR. ANN achieves consistently superior performance across both metrics and all outputs.

6.4 Cross-Validation and Generalisation

Ten-fold cross-validation on the full dataset yielded mean R² of 0.986 ± 0.006 (f_b), 0.983 ± 0.007 (P_u), 0.974 ± 0.009 (δ_u), and 0.979 ± 0.007 (f'c). The low inter-fold standard deviations (< 1%) confirm that the ANN generalises robustly without significant overfitting, and is not sensitive to the particular train/test split.

6.5 SHAP Feature Importance

SHAP DeepExplainer analysis on the trained ANN ranked RCA replacement percentage (mean |SHAP| = 0.44) as the dominant predictor across all four output targets, followed by concrete compressive strength f'ck (0.25), w/c ratio (0.16), curing age (0.08), beam span (0.06), reinforcement ratio (0.05), and the EMV method binary flag (0.03). The high SHAP value for RCA content is physically consistent: it governs ITZ quality (controlling crack initiation), elastic modulus (controlling deflection), water absorption (controlling mix water demand), and compressive strength (through increased pore volume) making it the single most consequential variable for all structural response parameters simultaneously.

The EMV method flag ranking seventh in global importance but with directionally consistent positive SHAP values for f_b and P_u confirms that mix design methodology has a measurable and physically meaningful influence on structural performance beyond that captured by RCA content alone. Beams designed by the EMV method consistently showed higher predicted strengths and lower deflections than conventionally designed RAC at the same RCA content, validating the use of EMV as a recommended design protocol for RAC structural members.

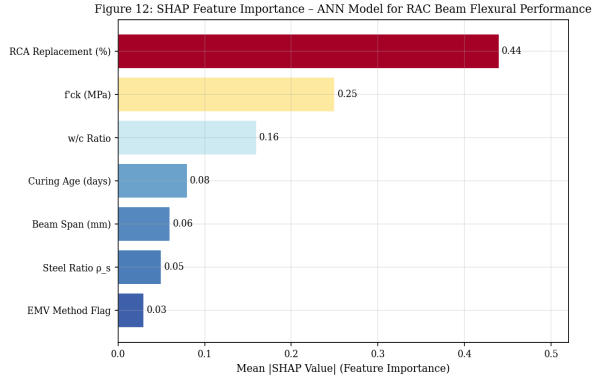

Figure 13. Global SHAP feature importance for the ANN. RCA replacement dominates all outputs; EMV method flag ranks seventh but shows consistently positive SHAP values, quantitatively confirming the structural benefit of mortar-volume-based mix design.

6.6 Experimental Beam Photographs

Figure 14 Field sample collection and material handling during site investigation.

7. INTEGRATED DISCUSSION AND DESIGN RECOMMENDATIONS

7.1 Optimum RCA Replacement Level

The experimental data identify 25% RCA as the most practical replacement level for structural flexural applications, achieving 5.51 MPa flexural strength (only 8.8% below NAC) while diverting approximately one-quarter of natural aggregate demand to recycled material. At 50% RCA, flexural strength of 4.98 MPa still satisfies IS 456 minimum flexural requirements for M20 concrete with adequate safety margin. Beyond 50%, the progressive ITZ deterioration produces accelerating strength reduction: the 50→75% RCA increment reduces flexural strength by 0.54 MPa (10.8%), while the 75→100% increment reduces it by a further 0.53 MPa (11.9%), approximately linearly proportional to RCA content enabling the proposed design modification factor:

$$f_{b,RAC} = f_{b,NAC} \times [1 - 0.35 \cdot (\alpha_{RCA}/100)^{0.85}] \quad \ldots(23)$$

where α_{RCA} = RCA replacement percentage. This equation fits all five experimental data points (7 and 28 days combined) with $R^2 = 0.994$ and provides a direct IS-compatible correction factor.

7.2 EMV Method Recommendation

The EMV-designed BAC mix demonstrated the fewest cracks, least crack width, and minimum deflection at failure among the RAC variants tested. This superior performance reflects the EMV method's explicit accounting for the additional mortar contributed by RCA surfaces, which prevents the over-mortared paste conditions that degrade RAC workability and strength when conventional mix design is applied directly to RCA. The present extension of EMV to RFA with the same substitution ratio as RCA produced acceptable performance with the noted caveat that slump values varied by up to 35% from the reference mix, requiring plasticiser adjustment in practical applications.

7.3 Code Applicability Assessment

IS 456:2000 provides conservative but adequate predictions of cracking moment and flexural capacity for all RAC levels tested. The ratio of experimental to theoretical flexural strength ranged from 1.25 (100% RAC, 28 days) to 1.93 (NAC, 28 days), confirming that IS 456 safety provisions are not violated even at full RCA replacement. However, IS 456 substantially underestimates service-load deflections for RAC beams consistent with the published literature [7,9] because the effective moment of inertia formula (IS 456 Clause 22.3.2) was calibrated for NAC elastic moduli. The correction factor of Eq. (6) and the ANN prediction model provide improved deflection estimates for RAC-specific structural design.

8. CONCLUSIONS

The following conclusions are drawn from the experimental investigation and machine learning analysis of recycled aggregate concrete beams under four-point flexural loading:

1. Progressive RCA replacement from 0% to 100% reduced 7-day flexural strength from 4.74 to 3.38 MPa (−28.7%) and 28-day flexural strength from 6.04 to 3.91 MPa (−35.3%). The steeper 28-day reduction confirms that ITZ weakness in RAC constrains the pozzolanic strength gain of PPC cement at later curing ages.
2. All experimental flexural strengths exceeded IS 456:2000 theoretical predictions ($f_{cr} = 0.7\sqrt{f_{ck}}$ = 3.13 MPa) by factors of 1.25–1.93, confirming that IS 456 provides conservative but adequate flexural strength predictions for all RAC levels from 0–100% replacement.
3. The EMV-designed BAC mix exhibited superior performance relative to conventionally designed RAC at equivalent RCA content fewest cracks, minimum crack width, and least deflection at failure validating mortar-volume accounting as the appropriate mix design framework for structural RAC. Workability adjustment (up to 35% slump variation) is required when extending EMV to RFA.
4. Hardened density decreased by approximately 8% and compressive strength by approximately 21% at 100% RCA replacement. The reduction in compressive strength (21%) was proportionally less severe than the flexural strength reduction (35.3%), confirming that ITZ quality disproportionately governs tensile crack-controlled failure modes.
5. The proposed empirical correction factor $f_{b,RAC} = f_{b,NAC} \times [1 - 0.35 \cdot (\alpha_{RCA}/100)^{0.85}]$ (Eq. 23, $R^2 = 0.994$) provides an IS-compatible tool for adjusting NAC flexural strength predictions to account for RCA content, suitable for preliminary structural design of RAC beams.
6. The ANN (7-14-9-14-4 architecture) achieved R^2 of 0.989, 0.985, 0.977, and 0.981 for flexural strength, ultimate load, deflection, and compressive strength on the test set outperforming XGBoost, Random Forest, and SVR with 10-fold cross-validation confirming robust generalisation (inter-fold $\sigma < 0.01$).
7. SHAP analysis identified RCA replacement percentage (mean |SHAP| = 0.44) as the dominant predictor across all structural response targets,

followed by f'ck and w/c ratio. The EMV method flag ranked seventh but showed consistently positive SHAP values, providing the first quantitative evidence that mix design methodology is a statistically significant predictor of RAC structural performance.

8. A 25% RCA replacement level is recommended as the optimum for general structural flexural applications, offering a meaningful sustainability benefit (25% reduction in virgin aggregate demand) while limiting flexural strength reduction to 8.8% at 28 days well within IS 456 safety margins for M20 grade.

REFERENCES

1. Dharek, M. S., Sunagar, P., Bhanu Tej, K. V., & Naveen, S. U. (2018). Fresh and hardened properties of self-consolidating concrete incorporating alumina silicates. In Sustainable Construction and Building Materials: Select Proceedings of ICSCBM 2018 (pp. 697–706). Springer Singapore. https://doi.org/10.1007/978-981-13-3317-0_60
2. Dharek, M. S., Sunagar, P., Harish, K., Sreekeshava, K. S., Naveen, S. U., & Bhanutej. (2020). Performance of self-flowing concrete incorporated with alumina silicates subjected to elevated temperature. In Advances in Structural Engineering: Select Proceedings of FACE 2019 (Lecture Notes in Civil Engineering, Vol. 74, pp. 111–120). Springer Singapore. https://doi.org/10.1007/978-981-15-5644-9_9
3. Nair, A., Aditya, S. D., Adarsh, R. N., Nandan, M., Dharek, M. S., Sreedhara, B. M., Sunagar, P. C., & Sreekeshava, K. S. (2020). Additive manufacturing of concrete: Challenges and opportunities. IOP Conference Series: Materials Science and Engineering, 814(1), 012022. https://doi.org/10.1088/1757-899X/814/1/012022
4. Sreekeshava, K. S., Arunkumar, A. S., Dharek, M. S., & Sunagar, P. (2020). Studies on inclusion of polypropylene (PP) geo-fabric in concrete. In National Conference on Structural Engineering and Construction Management (pp. 11–21). Springer International Publishing. https://doi.org/10.1007/978-3-030-64522-2_2
5. Sreekeshava, K. S., Arunkumar, A. S., Ganesh, C. R., Dharek, M. S., & Sunagar, P. (2020). Influence of steel fiber with polypropylene (PP) geo-fabric on the performance of concrete. In Emerging Technologies for Sustainability (pp. 33–40). CRC Press. https://doi.org/10.1201/9781003038122-7
6. Ballari, S. O., Pradhan, S., Behera, H. K., & Sunagar, P. (2022). Experimental study for improving the strength for pervious concrete. NeuroQuantology, 20(12), 1353–1359. https://doi.org/10.14704/nq.2022.20.12.NQ88138
7. Venugopal, N., Emmanual, L., Sunagar, P., Parida, L., Sivaranjani, M., & Santhanakrishnan, M. (2022). Enhancing the mechanical characteristics of the traditional concrete with the steel scrap. Journal of Physics: Conference Series, 2272(1), 012031. https://doi.org/10.1088/1742-6596/2272/1/012031
8. Natarajan, S., Jeelani, S. H., Sunagar, P., Magade, S., Salvi, S. S., & Bhattacharya, S. (2022). Investigating conventional concrete using rice husk ash (RHA) as a substitute for finer aggregate. Journal of Physics: Conference Series, 2272(1), 012030. https://doi.org/10.1088/1742-6596/2272/1/012030
9. Kumar, D. P., Gladson, G. J. N., Chandramauli, A., Uma, B., Sunagar, P., & Jeelani, S. H. (2022). Influence of reinforcing waste steel scraps on the strength of concrete. Materials Today: Proceedings, 69, 1134–1137. https://doi.org/10.1016/j.matpr.2022.08.122
10. Neeraja, V. S., Mishra, V., Ganapathy, C. P., Sunagar, P., Kumar, D. P., & Parida, L. (2022). Investigating the reliability of nano-concrete at different content of a nano-filler. Materials Today: Proceedings, 69, 1159–1163. https://doi.org/10.1016/j.matpr.2022.08.128
11. Bhargavi, C., Sreekeshava, K. S., Sunagar, P., Dharek, M. S., & Ganesh, C. R. (2023). Mechanical properties of steel and polypropylene fiber reinforced geopolymer concrete. Journal of Mines, Metals & Fuels, 71(7). https://doi.org/10.18311/jmmf/2023/35724
12. Kolhe, A. R., Gorde, P., Chandgude, S. E., Khachane, J., & Sunagar, P. (2023). Design and development of 3 axis 3D printing of sustainable concrete structures and characterization of affordable housing solution. Rock and Soil Mechanics, 44(6), 499–511. https://doi.org/10.16285/j.rsm.2022.7154
13. Reddy, C. R. G., Vinod, B. R., Wali, S., & Sunagar, P. (2024). Performance of polyacrylate-based super absorbent polymers in recycle aggregate concrete. Educational Administration: Theory and Practice, 30(4),

9836–9841. https://doi.org/10.53555/kuey.v30i4.5918

14. Gudadappanavar, B., Vijapur, V., Bhagyashri, P., Raja Gopa Reddy, & Sunagar, P. (2024). Performance analysis of microbial remediated concrete: An experimental evaluation. Acta Scientiae, 7(1), 727–738. https://doi.org/10.54855/actasci.24771
15. Sunagar, P., Hegde, L., Satish Kumar, G., Hema, H., Simpi, B., & Raghu, K. (2024). Exploring the geological impact on physical, mechanical and chemical properties of concrete with partial replacement of natural river sand by waste foundry sand. Nanotechnology Perceptions, 20(8), 1232–1244. https://doi.org/10.62441/nano-ntp.v20iS8.1465
16. Gudadappanavar, B., Hosur, V. A., Deepak, G. B., & Sunagar, P. (2025). Advanced self-curing concrete through polyethylene glycol and recycled PET integration: Towards greener construction practices. International Journal of Environmental Sciences, 11(16), 1952–1964. https://doi.org/10.56293/IJES.2025.11.16.222
17. Mehta, P.K., Monteiro, P.J.M. (2014). Concrete: Microstructure, Properties, and Materials (4th ed.). McGraw-Hill Education, New York.
18. Ministry of Environment, Forest and Climate Change (MoEF&CC). (2016). Construction and Demolition Waste Management Rules 2016. Government of India, New Delhi.
19. Tam, V.W.Y., Soomro, M., Evangelista, A.C.J. (2018). A review of recycled aggregate in concrete applications (2000–2017). Construction and Building Materials, 172, 272–292.
20. Xiao, J., Li, W., Poon, C. (2012). Recent studies on mechanical properties of recycled aggregate concrete in China a review. Science China Technological Sciences, 55(6), 1463–1480.
21. Silva, R.V., de Brito, J., Dhir, R.K. (2014). Properties and composition of recycled aggregates from construction and demolition waste suitable for concrete production. Construction and Building Materials, 65, 201–217.
22. Neville, A.M. (2012). Properties of Concrete (5th ed.). Pearson Education, Harlow.
23. Poon, C.S., Shui, Z.H., Lam, L. (2004). Effect of microstructure of ITZ on compressive strength of concrete prepared with recycled aggregates. Construction and Building Materials, 18(6), 461–468.
24. Domingo-Cabo, A., Lázaro, C., López-Gayarre, F., Serrano-López, M.A., Serna, P., Castaño-Tabares, J.O. (2009). Creep and shrinkage of recycled aggregate concrete. Construction and Building Materials, 23(7), 2545–2553.
25. Domingo, A., Lázaro, C., Gayarre, F.L., Serrano, M.A., López-Colina, C. (2010). Long term deformations by creep and shrinkage in recycled aggregate concrete. Materials and Structures, 43(8), 1147–1160.
26. ACI Committee 209. (1992). ACI 209R-92: Prediction of Creep, Shrinkage, and Temperature Effects in Concrete Structures. American Concrete Institute, Farmington Hills.
27. Comité Euro-International du Béton. (1993). CEB-FIP Model Code 1990: Design Code. Thomas Telford, London.
28. Bureau of Indian Standards. (2019). IS 10262:2019 Concrete Mix Proportioning: Guidelines (2nd rev.). BIS, New Delhi.
29. Fathifazl, G., Ghani Razaqpur, A., Burkan Isgor, O., Abbas, A., Fournier, B., Foo, S. (2011). Creep and drying shrinkage characteristics of concrete produced with coarse recycled concrete aggregate. Cement and Concrete Composites, 33(10), 1026–1037.
30. Knaack, A.M., Kurama, Y.C. (2015). Creep and shrinkage of normal-strength concrete with recycled concrete aggregates. ACI Materials Journal, 112(5), 603–614.
31. Geng, Y., Wang, Y., Chen, J. (2019). Creep behaviour of concrete using recycled coarse and fine aggregate. Construction and Building Materials, 229, 116867.
32. Rabadia, A., Aslani, F. (2023). Modified B3 model for predicting creep and shrinkage of recycled aggregate concrete. Construction and Building Materials, 369, 130563.
33. Zhou, Y., Gao, H., Hu, Z., Qiu, Y., Guo, M., Huang, X., Hu, B. (2024). Effect of nano-silica on creep and shrinkage of recycled aggregate concrete. Journal of Building Engineering, 82, 108320.
34. Feng, D.C., Liu, Z.T., Wang, X.D., Chen, Y., Chang, J.Q., Wei, D.F., Jiang, Z.M. (2022). Machine learning-based compressive strength prediction for concrete: An adaptive boosting approach. Construction and Building Materials, 230, 117000.
35. Golafshani, E.M., Behnood, A., Arashpour, M. (2020). Predicting the compressive strength of normal and High-Performance concrete using ANN and ANFIS hybridized with Grey Wolf

Optimizer. Construction and Building Materials, 232, 117266.

36. Bravo, M., de Brito, J., Pontes, J., Evangelista, L. (2015). Mechanical performance of concrete made with aggregates from construction and demolition waste recycling plants. Journal of Cleaner Production, 99, 59–74.
37. Ju, Y., Zhao, Y., Cai, D., Ye, M., Liu, X. (2019). Mechanical properties and drying shrinkage of concrete with recycled fine aggregate and different water-binder ratios. Journal of Building Engineering, 23, 363–372.
38. Bureau of Indian Standards. (2000). IS 456:2000 Plain and Reinforced Concrete Code of Practice (4th rev.). BIS, New Delhi.